Available online at www.sciencedirect.com
SCIENCE DIRECT®
Journal of Magnetic Resonance 165 (2003) 219–229
JMR Journal of Magnetic Resonance
www.elsevier.com/locate/jmr

Centric scan SPRITE magnetic resonance imaging

Meghan Halse, David J. Goodyear, Bryce MacMillan, Pavol Szomolanyi, David Matheson, and Bruce J. Balcom*

Department of Physics, MRI Centre, P.O. Box 4400, University of New Brunswick, Fredericton, NB, Canada E3B 5A3

Received 18 June 2003; revised 11 August 2003

Communicated by Joseph Ackerman

Abstract

Two rapid, pure phase encode, centric scan, Single Point Ramped Imaging with T_1-Enhancement (SPRITE) MRI methods are described. Each retains the benefits of the standard SPRITE method, most notably the ability to image short T_2^* systems, while increasing the sensitivity and generality of the technique. The Spiral-SPRITE method utilizes a modified Archimedean spiral k-space trajectory. The Conical-SPRITE method utilizes a system of spirals mapped to conical surfaces to sample the k-space cube. The sampled k-space points are naturally Cartesian grid points, eliminating the requirement of a re-gridding procedure prior to image reconstruction. The effects of transient state behaviour on image resolution and signal/noise are explored.

Keywords: MRI; Materials; Short T_2^*; SPRITE; Spiral trajectory

1. Introduction

Single point imaging (SPI) MRI methods have proven to be a useful imaging modality for studies of short relaxation time systems [1–4]. Unlike frequency encoding, where the time evolution of magnetization is measured, SPI is a pure phase encode technique. Images acquired using SPI methods are free from artifacts due to B_0 inhomogeneity, chemical shift, and susceptibility variations [5]. In SPI radio frequency (RF) pulses are applied in the presence of the phase encode gradient, G, and a single point is acquired during the free induction decay (FID) at a time t_p commonly referred to as the encoding time. The acquisition is regarded as inefficient since only one k-space point is acquired for each gradient switch on/off. Any attempt to increase acquisition speed can result in excessive gradient vibration due to rapid gradient switching.

The SPRITE (Single Point Ramped Imaging with T_1 Enhancement) sequence [6], a development of SPI, employs ramped phase encode gradients which permits image acquisition at a greater speed and minimizes gradient vibration arising from impulsive Lorentz forces. The SPRITE sequence enables the introduction of T_1 contrast through partial saturation of magnetization components which have longitudinal relaxation times that are longer then the gradient switching time [6]. A wide variety of magnetization preparation techniques may be employed to control image contrast or permit relaxation time mapping. For example, Mastikhin et al. [7] have shown that SPRITE with centric half k-space sampling may be used to obtain images with T_1 and $T_{1\rho}$ weightings through magnetization preparation. Additionally, Beyea et al. [3] and Axelson et al. [8] have used SPI methods for relaxation time mapping of short T_2^* nuclei.

SPI sequences rely on non-selective broadband RF pulses. In order to obtain homogeneous excitation of the spin system, the duration of the pulses are limited by the maximum spectral width of the object ($G_{\max} \times$ sample length). In SPI this restriction calls for small RF flip angles and therefore, in some cases, requires extensive signal averaging to obtain acceptable S/N. This may be acceptable for systems where longitudinal relaxation times are sufficiently short. However, for materials with long T_1s, extensive averaging leads to prolonged

* Corresponding author. Fax: +1-506-453-4581.
E-mail address: bjb@unb.ca (B.J. Balcom).

1090-7807/$ - see front matter © 2003 Elsevier Inc. All rights reserved.
doi:10.1016/j.jmr.2003.08.004

acquisition times. Increasing acquisition speed results in excessive saturation of longitudinal magnetization which leads to low image intensity. Using a centric sampling acquisition scheme, the z-magnetization could be sampled more efficiently, permitting high quality image acquisition which is impossible for SPI. Mastikhin et al. [7] have shown that SPRITE with half k-space centric order sampling may be used to image long T_1 materials, with acceptable image acquisition times and S/N.

Since the development of SPRITE, the original methodology, we have considered alternate k-space trajectories to increase sensitivity (S/N and acquisition speed) of the technique. In this paper we outline two new pure phase encode centric sampling MRI acquisition strategies. Spiral-SPRITE [9] employs pure phase encode, centric sampling along a modified Archimedean spiral trajectory. The Spiral-SPRITE technique has been the subject of a recent conference publication [10] associated with the 5th International Meeting on Recent Advances in MR Applications to Porous Media. Conical-SPRITE [11], a 3D centric sampling technique, employs pure phase encoding with a system of spiral trajectories mapped to conical surfaces, to sample k-space. These techniques have several natural advantages: simplified image contrast, increased S/N, reduced acquisition times, and reduced gradient duty cycle, which are the subject of this communication.

Spiral k-space sampling has become a common pure frequency encode methodology in biomedical imaging. The nested cones trajectory has been suggested in conjunction with frequency encoding by Nishimura and Irarrazabal [12]. Frequency encode spiral trajectories require re-gridding of the experimental k-space data points prior to image reconstruction [13]. This data processing step is avoided in Spiral-SPRITE and Conical-SPRITE since the acquired k-space data points quite naturally fall on Cartesian grid points.

2. Theory

2.1. The spiral-SPRITE trajectory

Spiral-SPRITE is the foundation for Conical-SPRITE; therefore, we shall first present the Spiral-SPRITE trajectory and introduce a common notation for these centric scan techniques.

The traditional Archimedean spiral k-space trajectory in polar coordinates is given by

$$\mathbf{k}_r = a\theta\hat{\boldsymbol{k}}, \tag{1}$$

where θ is the polar angle measured with respect to the k_x-axis, a is a constant which defines the rate of change of the spiral trajectory and along the radial direction in k-space, and $\hat{\boldsymbol{k}}$ is the unit vector directed along $\mathbf{k}_r$. For constant radial sampling the derivative of $|\mathbf{k}_r|$ with respect to θ must be constant [14]. Nyquist sampling requires the interval along the radial direction of k-space, for M spiral interleaves and a given image field of view, FOV, to be

$$\Delta k_r = \frac{M}{\mathrm{FOV}}, \tag{2}$$

where the FOV can be defined as

$$2MN_r\Delta r = \mathrm{FOV} \tag{3}$$

and Δr is the nominal pixel resolution of the image [14,15]. Using the notation of Ahn et al. [15] we define N_r as the number of rotations of the spiral trajectory and N_θ is defined as the number of sampled points on one rotation of the spiral. The angular sampling interval along the k-space trajectory can be written as

$$\Delta\theta = \frac{2\pi}{N_\theta}. \tag{4}$$

The radial and angular k-space sampling intervals are depicted in Fig. 1. For the single point approach to spiral scan imaging, we use a formulation which is similar to that used for frequency encoding methods. We consider the construction of one spiral assuming that multiple interleaved spiral trajectories, if desired, can be determined through a rotation of coordinates. We allow for the possibility of spiral interleaves in the variable M. In this work M is always 1.

In Cartesian coordinates the k_x and k_y components of the spiral trajectory can be written as

$$\begin{aligned} k_x &= af_c(\theta), \\ k_y &= af_s(\theta), \end{aligned} \tag{5}$$

where $f_c(\theta)$ and $f_s(\theta)$ are functions defined by

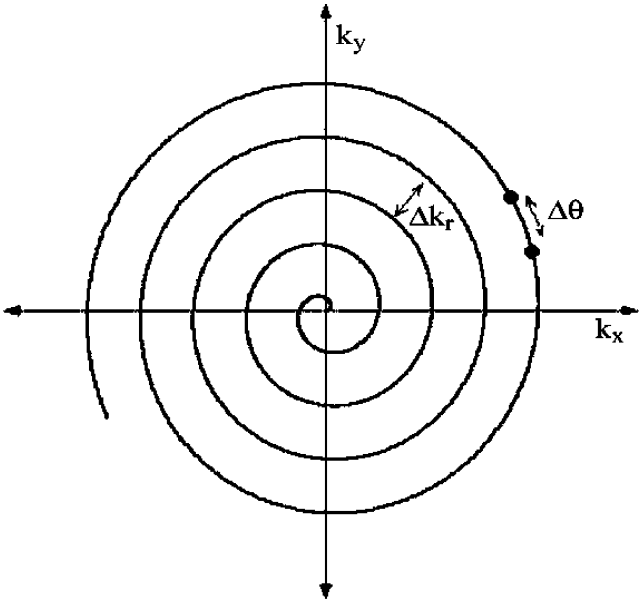

Fig. 1. An illustration of Spiral k-space sampling. The sampling interval Δk_r is the radial distance between consecutive rotations of the spiral trajectory. $\Delta\theta$ is the angular spacing between consecutively sampled k-space points, as defined by Eq. (4).

$$f_c(\theta) = \frac{\theta}{\theta_{\max}} \cos\theta,$$
$$f_s(\theta) = \frac{\theta}{\theta_{\max}} \sin\theta, \tag{6}$$

where $\theta_{\max}$ is the maximum angle of the trajectory which is dependent on the number of spiral rotations, N_r, of the spiral trajectory and the range of θ is such that

$$0 \leqslant \theta \leqslant \theta_{\max}, \quad \theta_{max} = 2\pi N_r. \tag{7}$$

The constant, $\theta_{\max}$, has been introduced so that the sum of the squares of the functions is equal to unity when evaluated at the last point on the spiral trajectory (i.e., at $\theta_{\max}$). This formulation leads to the determination of the constant a. At the extremity of k-space we find

$$k_{\max} = \sqrt{k_x^2 + k_y^2} = a. \tag{8}$$

However, $k_{\max} = N_r \Delta k_r$, which is just the number of spiral rotations multiplied by the k-space step in the radial direction. Using Eqs. (2)–(8), the spiral k-space coordinates can be further written as

$$k_x = \frac{M}{\mathrm{FOV}} \frac{\theta}{2\pi} \cos\theta,$$
$$k_y = \frac{M}{\mathrm{FOV}} \frac{\theta}{2\pi} \sin\theta. \tag{9}$$

For traditional spiral imaging techniques, the variable θ would be time dependent. It typically depends on hardware constraints such as gradient amplifier instantaneous peak current, slew rate, and RMS current, which determine the rate at which the spiral trajectory is traversed during data acquisition [14]. The constraints are important in conventional spiral imaging where spiral k-space trajectories permit acquisition of frequency encoded signals with long inherent T_2s using a minimal number of RF excitations. In spiral single point imaging, θ is also time dependent. However in Spiral-SPRITE the speed at which we scan k-space is not determined by the gradient amplifier slew rate. Instead the rate is governed by the magnetic field gradient rise time, or how fast phase encode gradients can be switched from one level to another, and the repetition time between gradient switches. At an arbitrary time t after the initial RF pulse the number of pulses can be written

$$n = \left[\left[\frac{t}{T_{\mathrm{R}}}\right]\right] + 1, \tag{10}$$

which is defined in terms of a nearest integer function. Here T_{R} is the repetition time between RF pulses. Each k-space point on the spiral trajectory corresponds to a single RF excitation of the sample with detection of a chosen FID point. The angle spanned after n pulses is given by

$$\theta = \left[\left[\frac{t}{T_{\mathrm{R}}}\right]\right] \frac{2\pi}{N_\theta} = (n-1)\Delta\theta. \tag{11}$$

Using Eqs. (9) and (11) we find that the k-space coordinates of the spiral trajectory after n pulses can be written as

$$k_x = 2\pi \frac{M}{\mathrm{FOV}} \frac{n-1}{N_\theta} \cos\left(\frac{2\pi(n-1)}{N_\theta}\right),$$
$$k_y = 2\pi \frac{M}{\mathrm{FOV}} \frac{n-1}{N_\theta} \sin\left(\frac{2\pi(n-1)}{N_\theta}\right). \tag{12}$$

We project the spiral coordinates onto a square equispaced $W \times W$ Cartesian grid where W is typically a power of 2 so the FFT may be employed for rapid image reconstruction. The range of k_x and k_y are defined by $|k_x| \leqslant k_{\max}$ and $|k_y| \leqslant k_{\max}$. We round (k_x, k_y) to nearest neighbour grid points $(\bar{k}_x, \bar{k}_y)$ given by

$$\bar{k}_x = \frac{\gamma}{2\pi} G_x t_p,$$
$$\bar{k}_y = \frac{\gamma}{2\pi} G_y t_p, \tag{13}$$

where γ is the nuclear gyromagnetic ratio, G_x and G_y are magnetic field gradient amplitudes, and t_p the encoding time. The magnetic field gradient amplitudes used for the spiral scan technique are then calculated using Eq. (12).

We now consider how one would choose N_r and the N_θ given that the final image will be on a square equispaced grid. Since we are assuming that the image has a final dimension of $W \times W$ with an equivalent field of view in each dimension, then the nominal resolution along the x- or y-directions of the image is simply the FOV divided by the number of points along one dimension of the grid. Using Eq. (3) the approximate number of spiral rotations for a given number of spiral interleaves is

$$N_r = \frac{W}{2M}. \tag{14}$$

In order to determine N_θ we consider the following argument. The spiral trajectory, including interleaves, lies within a circle with radius $k_{\max}$ centered on the origin. The ratio of the circular area to the area of the square k-space grid is

$$\frac{\pi k_{\max}^2}{(2k_{\max})^2} \approx \frac{3}{4}. \tag{15}$$

The total number of spiral points, including the points from spiral interleaving, is $M \times N$ and would be contained within the circular area. The ratio of the total number of spiral points to the total grid points is approximately equal to the ratio of the areas presented in Eq. (15). For an equally spaced grid the approximate number of grid points contained within the circular area is therefore

$$MN = \frac{3}{4} W^2 \tag{16}$$

and since $N = N_r N_\theta$ is the total number of spiral points we find that the number of points per spiral rotation

which would be equivalent to the number of points contained in the circular area is

$$N_\theta = \frac{3}{4}\frac{W^2}{MN_r}. \tag{17}$$

This provides an approximate value for the number of points per spiral rotation.

The Spiral-SPRITE trajectory is similar to SPRITE phase encoding which consists of a set of equally incremented discrete gradient steps [6]. However, for Spiral-SPRITE the G_x and G_y gradients are sinusoidally ramped through a set of discrete gradient steps as illustrated in the pulse sequence presented in Fig. 2. The trajectory is reminiscent of the pure frequency encoding square spiral trajectory presented by Meyer et al. [16].

2.2. The conical-SPRITE trajectory

The spiral trajectory is a natural 2D k-space sampling method. The extension to 3D requires an additional phase encode gradient in the third dimension. The resulting 'stack of spirals' trajectory does not begin sampling in the centre of the k-space cube for all spirals and is therefore not a true 3D centric scanning technique. We may avoid this difficulty by generating a spiral trajectory which is mapped onto a conical surface to explore the third dimension of k-space. (Fig. 3) This is accomplished by extending the Archimedean spiral with the addition of a θ dependent component in the z-dimension

$$\mathbf{k} = a\theta\hat{k}_r + b\theta\hat{k}_z. \tag{18}$$

This cone can be described by a pitch angle, ϕ, and a radius, R. The pitch angle is defined by the inverse tangent of the ratio of the constants, a and b. The radius is given by the square root of the sum of the squares of a and b. A nested system of these cones can be defined such that the overall trajectory inscribes a sphere in the k-space cube. The constants a_n and b_n for each of the N_c nested cones are given by

$$a_n = \frac{R\tan\phi_n}{\sqrt{1-\tan^2\phi_n}},$$
$$b_n = \frac{\tan\phi_n}{\sqrt{1-\tan^2\phi_n}}, \tag{19}$$

where the pitch angle for each cone is

$$\phi_n = \frac{(n-1)\pi}{(N_c-1)}, \quad n = 1, 2, \ldots, N_c$$

and the radius is a constant which describes the largest sphere which can be inscribed within the k-space cube

$$R = \frac{k_{\max}}{2}.$$

For illustrative purposes, a system of three nested cones is shown in Fig. 4.

Maintaining the notation used above for Spiral-SPRITE, the Cartesian coordinates for the Conical-SPRITE trajectory are

$$k_x = a_n\frac{\theta}{\theta_{\max}}\cos\theta,$$
$$k_y = a_n\frac{\theta}{\theta_{\max}}\sin\theta,$$
$$k_z = b_n\frac{\theta}{\theta_{\max}}.$$

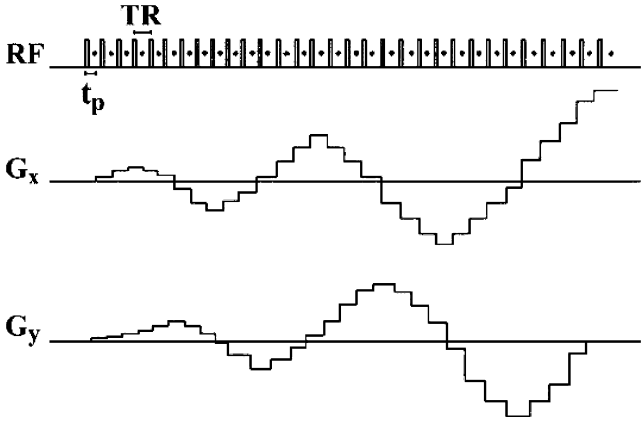

Fig. 2. The Spiral-SPRITE pulse sequence. Each gradient step corresponds to a sample excitation using a broadband RF pulse. The gradients are sinusoidally ramped through a discrete set of gradient amplitudes for each spiral interleave. This diagram is illustrative of a single spiral interleave.

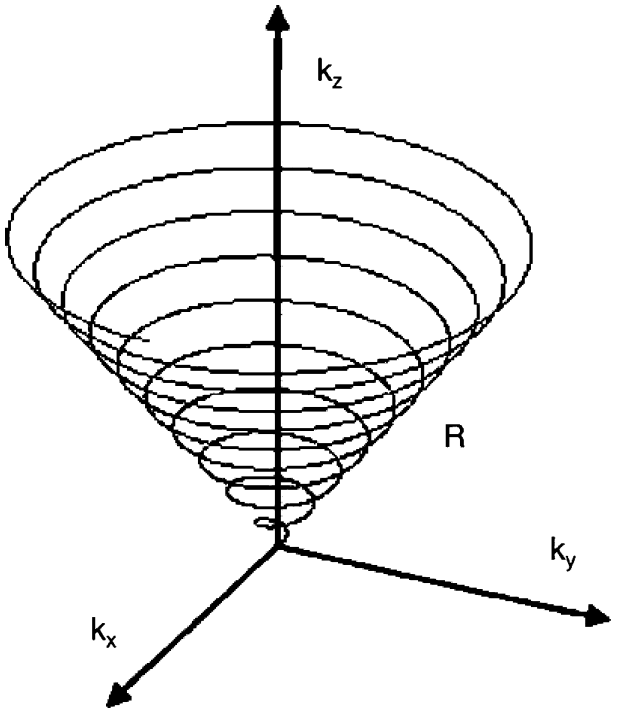

Fig. 3. A single spiral mapped to a conical surface. This conical trajectory can be classified by a radius, R, defined as the length of the side of the cone and a pitch angle, ϕ, defined as the angle between the central k_z-axis and the surface of the cone.

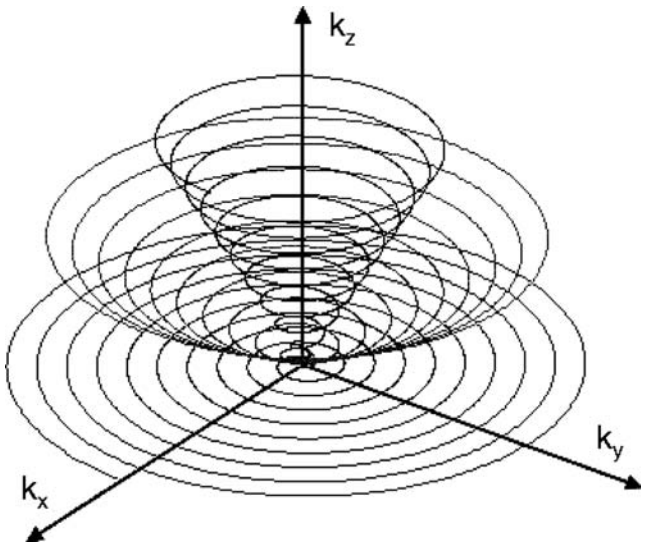

Fig. 4. A system of three conical trajectories nested to form the top half of a sphere in k-space. Three cones are chosen for ease of illustration. In practice 39 cones are implemented for 3D Conical-SPRITE.

Using Eq. (11) we can write the Cartesian coordinates after n pulses

$$k_x = a_n \frac{(n-1)}{N_r N_\theta} \cos\left(\frac{2\pi(N-1)}{N_\theta}\right),$$
$$k_y = a_n \frac{(n-1)}{N_r N_\theta} \sin\left(\frac{2\pi(N-1)}{N_\theta}\right), \qquad (20)$$
$$k_z = b_n \frac{(n-1)}{N_r N_\theta}.$$

As with the spiral trajectory, we project the conical coordinates onto a cubic equispaced $W \times W \times W$ Cartesian grid where W is typically a power of 2 so the FFT may be employed for rapid image reconstruction. The range of k_x, k_y, and k_z are defined by $|\bar{k}_x| \leqslant k_{\max}$, $|\bar{k}_y| \leqslant k_{\max}$, and $|\bar{k}_z| \leqslant k_{\max}$. The magnetic field gradient amplitudes used for the Conical-SPRITE scan technique are then calculated using Eqs. (19) and (20).

The parameters N_c, N_r, and N_θ are chosen with consideration given to the previous knowledge that the trajectory will be projected onto a cubic equispaced grid and to the desired values for the total number of points in the final trajectory, and the maximum number of points acquired along a single conical trajectory.

The total number of points acquired by this acquisition strategy is proportional to the volume of the sphere inscribed within the k-space cube. The ratio of the volume within the sphere defined by the nested cones trajectory to the volume of the entire k-space cube is

$$\frac{\left(\frac{4}{3}\pi R^3\right)}{(2R)^3} \approx \frac{1}{2}.$$

Therefore the total number of points acquired by the conical SPRITE method has an upper bound of approximately $1/2W^3$.

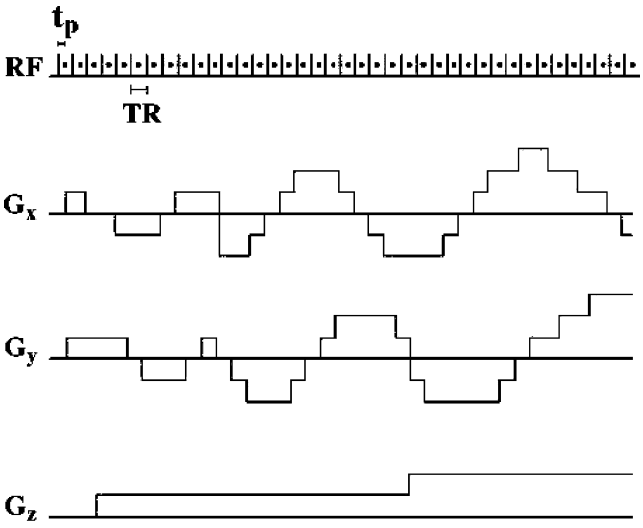

Fig. 5. The 3D Conical-SPRITE pulse sequence. G_x and G_y are sinusoidally ramped while G_z is linearly ramped through a discrete set of gradient amplitudes for each nested cone. The first point on each cone is acquired in the absence of any gradients. This diagram is illustrative of the first few dozen points on a single conical trajectory.

The maximum number of points in a single conical acquisition is limited by gradient duty cycle and longitudinal magnetization evolution considerations.

The pulse sequence diagram for Conical-SPRITE is depicted in Fig. 5. The x and y gradients vary sinusoidally, reminiscent of the Spiral-SPRITE sequence, while the z gradient is a stepped linear ramp.

In both Spiral-SPRITE and Conical-SPRITE, the rounding of points to the equispaced square or cubic grid results in duplication of some of the Cartesian grid points, especially near the centre of k-space where sampling is denser. Duplicate points are not acquired, with consequent modifications to the gradient waveform, except in the case of duplicate points which are acquired after the same number of RF pulses on adjacent cones or spiral interleaves. In this case the duplicate points have the same longitudinal magnetization saturation weighting and are signal averaged.

3. Experimental

The Conical-SPRITE sequence was implemented on a Nalorac (Martinez, CA) 2.4 T 32 cm i.d. horizontal bore superconducting magnet with a water cooled 7.5 cm i.d. gradient set (maximum gradient strength 100 G/cm) driven by Techron (Elkhart, IN) 8710 amplifiers. The ^{1}H RF probe was a ^{1}H free 32 rung quadrature birdcage coil (Morris Instruments, Ottawa). The ^{19}F RF probe was a homemade 8 rung birdcage quadrature coil. The probes were driven by a 2 kW AMT (Brea, CA) 3445 RF amplifier. The console was a Tecmag (Houston, TX) Apollo. All experiments were performed at ambient temperature.

The Cartesian components of the generic Spiral-SPRITE and Conical-SPRITE gradient waveforms, with gradient values between the arbitrary limits ± 100, were calculated and loaded onto the Apollo console. The generic waveform provided a template which could be linearly scaled in amplitude by the console according to the specific imaging parameters, t_p and FOV, for a given experiment. The template conical k-space trajectory, used for all the Conical-SPRITE experiments, was constructed using IDL version 5.5 (Research Systems, Boulder, CO). The number of nested cones was chosen to be $N_c = 39$, the number of k-space rotations for each conc was $N_r = 40$. The total number of points acquired for the 3D 64^3 images was 61 690 while the maximum number of points on a single k-space cone was 2242.

The ^{19}F sample was a Teflon sleeve with a diameter of 38 mm and a length of 89 mm. The relaxation times of the sample were $T_1 = 150$ ms and $T_2* = 35\,\mu$s. The Teflon sleeve image was acquired with $t_p = 30\,\mu$s, FOV $= 8\,\text{cm} \times 8\,\text{cm} \times 20\,\text{cm}$, $T_R = 2$ ms, flip angle $= 8°$ in 16 averages. The total image acquisition time for the 3D 64^3 image was 40 min.

The ^{1}H resolution phantom was a crosslinked *cis*-polybutadiene disk. The dimensions of the disk are presented in Fig. 7. The relaxation times for this sample were $T_1 = 218$ ms and $T_2^* = 330\,\mu$s. Images of the resolution phantom were acquired with $t_p = 100\,\mu$s, FOV $= 6\,\text{cm} \times 6\,\text{cm} \times 6\,\text{cm}$, $T_R = 2$ ms, 4 averages and flip angles of 4.6°, 6.5°, 9.1°, and 13.1°. The total acquisition time for each 3D 64^3 image was 12 min and 40 s.

The second ^{1}H imaging sample was a 3 cm long water saturated concrete sample with a diameter of 2 cm. The longitudinal relaxation time of the water within the concrete was approximately 1 ms with a T_2^* of approximately 150 μs. The water saturated concrete images were acquired with $tp = 80\,\mu$s, FOV $= 6\,\text{cm} \times 6\,\text{cm} \times 6\,\text{cm}$, flip angle $= 34°$ in a single scan. The first 3D 64^3 image was acquired with $T_R = 2$ ms in 2 min and 18 s. The second 3D 64^3 image was acquired with $T_R = 250\,\mu$s in 33 s.

S/N for all images was calculated as a ratio of the mean image intensity of a region of interest within the sample area compared to the mean image intensity from a similar region of the background.

Point spread functions were numerically simulated using IDL version 5.5 (Research Systems, Boulder, CO).

4. Results/discussion

4.1. Centric scan signal equation

The original SPRITE technique is a longitudinal steady-state imaging method [6,7]. A dynamic approach to equilibrium is achieved by applying low flip angle RF pulses while initially sampling at the edge of k-space where the observed MR signal is relatively small. The observed image intensity at any point in the image is related to the equilibrium longitudinal magnetization through

$$S = M_0 e^{-t_p/T_2^*} \left| \frac{1 - e^{-T_R/T_1}}{1 - \cos\theta e^{-T_R/T_1}} \right| \sin\theta, \tag{21}$$

where the exponential factor containing T_2^* accounts for magnetization de-phasing after the application of the RF pulse [6,17]. This particular aspect of SPRITE has been investigated experimentally and analytically by Mastikhin et al. [7] and Prado et al. [4]. The approach to steady state through application of multiple RF pulses has been described by Vlaardingerbroek and den Boer [18].

The centric scan SPRITE techniques may be employed to utilize longitudinal magnetization more efficiently, especially for materials which exhibit long spin–lattice relaxation times (on the order of hundreds of milliseconds). For $T_R \ll 5T_1$ the successive application of RF pulses leads to saturation of z-magnetization. However, in the case of a centric scan SPRITE technique there is no z-magnetization saturation of the central k-space point. Therefore for a centric scan SPRITE experiment the local image intensity at any point in the image is related to the equilibrium longitudinal magnetization through

$$S = M_0 e^{-t_p/T_2^*} \sin\theta. \tag{22}$$

Fig. 6 shows a 3D rendered Conical-SPRITE image of a Teflon sleeve with $T_2^* = 35\,\mu$s and $T_1 = 150$ ms. This image demonstrates the viability of the use of Conical-SPRITE for acquiring high quality images, in reasonable acquisition times, of samples with short T_2^* and longer T_1 (hundreds of milliseconds). The S/N for this image was 10.5. If a similar image was acquired with standard SPRITE the S/N would be reduced by 42% due to longitudinal magnetization saturation effects.

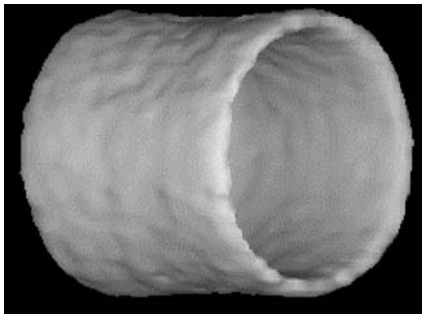

Fig. 6. A ^{19}F Conical-SPRITE image of a Teflon sleeve acquired with a t_p of 30 μs, FOV of $8\,\text{cm} \times 8\,\text{cm} \times 20\,\text{cm}$, T_R of 2 ms, flip angle of 8° with 16 averages. The total image acquisition time for the 3D 64^3 image was 40 min. The relaxation times of this sample are $T_1 = 150$ ms and $T_2^* = 35\,\mu$s. The image S/N was 10.5.

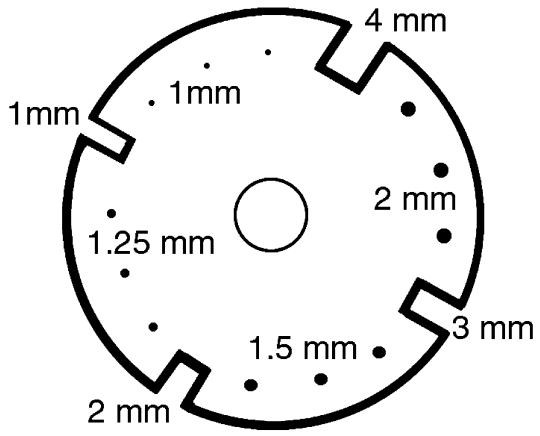

Fig. 7. A schematic diagram of the resolution phantom employed in Fig. 8.

The signal equation, Eq. (22), was further explored through the acquisition of Conical-SPRITE images of a ^{1}H resolution phantom at four different RF flip angles. 2D slices from these 3D images are presented in Fig. 8. Increasing the applied RF flip angle (4.6°, 6.5°, 9.1°, 13.1°) leads to an increased S/N, according to the $\sin\theta$ term in the signal equation.

The centric scan SPRITE techniques are naturally density weighted. The signal equation, Eq. (22), suggests that the available transverse magnetization at any given point in the image is proportional to the equilibrium magnetization, and thus the nuclei density, reduced only by the transverse magnetization dephasing term, controlled by the choice of t_p/T_2^*, and the sine of the flip angle. The relationship between the signal intensity and the sine of the flip angle can be verified from the proton resolution phantom images in Fig. 8. The signal to noise in the first image, acquired with a flip angle of 4.6°, was calculated to be 25. The S/N calculated from the last image, acquired with a flip angle of 13.1°, was 78. The ratio of the sine of the flip angles of these images is 2.8. The ratio of the S/N of these images is 3.1. This demonstrates the validity of the relationship between signal and flip angle as presented by the signal equation (Eq. (22)). The degradation of image resolution with increasing flip angle, which is also apparent in Fig. 8, will be discussed later in this manuscript.

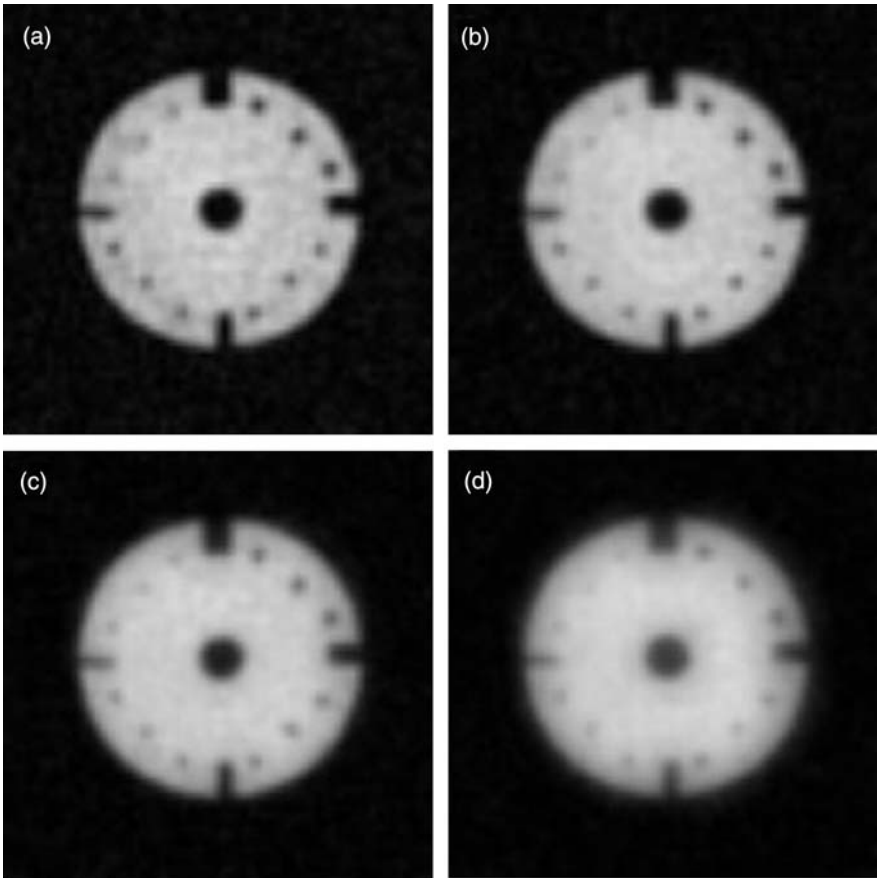

Fig. 8. 2D slices from 3D ^{1}H Conical-SPRITE images of a crosslinked *cis*-polybutadiene resolution phantom. Images were acquired with a t_p of 100 μs, an isotropic FOV of 6 cm × 6 cm × 6 cm, T_R of 2 ms with 4 averages. The total acquisition time for each 3D 64^3 image was 12 min and 40 s. The flip angles employed were (a) 4.6°, (b) 6.5°, (c) 9.5°, and (d) 13.1°.

4.2. Rapidity of data acquisition

Image acquisition times are significantly decreased with Spiral-SPRITE and Conical-SPRITE compared to conventional SPRITE imaging. This arises from two combined effects. First, the corners of k-space, where signal intensity is typically low and where minimal contributions to the image features are anticipated, are naturally omitted from the centric scan trajectories. This reduces the number of acquired points, and consequently the acquisition time, to approximately $3/4$ in the case of Spiral-SPRITE (Eq. (15)) and $1/2$ in the case of Conical-SPRITE compared to the standard SPRITE case. Second, the number of spiral interleaves or nested cones is typically less than the number of analogous lines acquired in conventional SPRITE imaging. This saves acquisition time on the delays between lines for magnetization recovery and gradient cooling.

In the case of samples with a short spin–lattice relaxation time (on the order of milliseconds), image acquisition times can be significantly reduced because T_R for the experiment can be greatly reduced without significant image resolution loss. The first 64^3 3D ^{1}H Conical-SPRITE image of the water saturated concrete sample (Fig. 9a) was acquired with $T_R = 2$ ms in 2 min and 18 s and had a S/N of 14. The second image (Fig. 9b) was acquired with a T_R of 250 μs in 33 s and had a S/N of 12. The reduction in total imaging time is not in proportion to the T_R reduction because of other delays in the pulse sequence, which have been maintained constant. Most notable is the time delay between sequential cones.

The T_R in the second image, 250 μs, is on the order of the switching time of the gradients. This introduces an uncertainty in the gradient values at the time of acquisition, and consequently the value of the k-space point acquired. Despite the uncertainty in true k-space coordinates, which will degrade image resolution, a high quality image is still acquired. The shorter T_R of the second image would reduce the image intensity, with a standard SPRITE acquisition, by approximately 40% according to Eq. (21). The observed S/N of the two images is however minimally different. This result upholds the centric scan signal equation (Eq. (22)) and illustrates the increased sensitivity of the centric scan SPRITE techniques over the standard SPRITE method.

4.3. Gradient duty cycle

Our two new centric scan SPRITE acquisition strategies have a significantly reduced gradient duty cycle compared to analogous standard SPRITE experiments. The overall duty cycle is much less because less time is spent acquiring points at the extremities of k-space where gradient values are typically very high. Relative duty cycles for Conical-SPRITE and standard SPRITE experiments can be calculated by summing the gradient values, ranging from −100 to 100, within the template gradient waveform for each technique over the period of interest, normalizing the result by the total number of gradient steps. The gradient duty cycle for a complete conventional SPRITE experiment is 50.8%. The gradient duty cycle for a complete Conical-SPRITE experiment is 29.7% for G_x and G_y, and 33.8% for G_z. On a smaller time scale, within a single experiment, gradient duty cycles for centric scan SPRITE techniques are greatly reduced by the ramping of the gradients in all three dimensions. In a conventional SPRITE experiment, the primary phase encode gradient is a linear ramp while the two secondary phase encode gradients are maintained at a constant value throughout the acquisition of a single line in k-space. Standard SPRITE

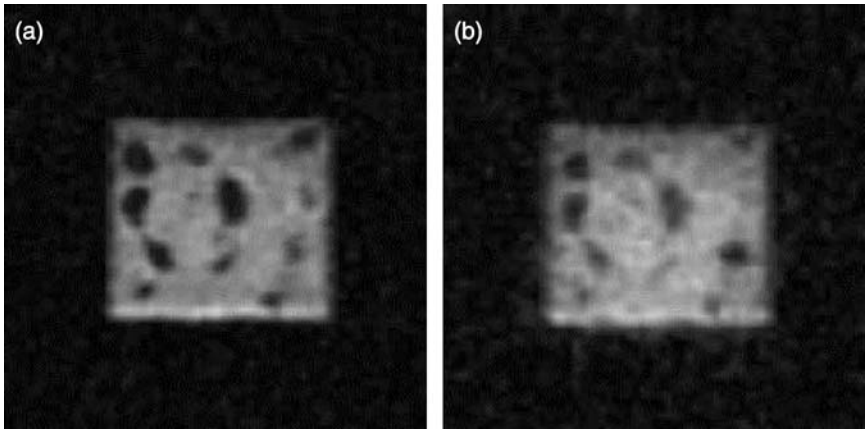

Fig. 9. (a) A 2D slice from a 3D ^{1}H Conical-SPRITE image of a water saturated concrete sample acquired with a t_p of 80 μs, an isotropic FOV of 6 cm × 6 cm × 6 cm, flip angle of 34°, and T_R of 2 ms in a single scan. The total acquisition time of this 3D 64^3 image was 2 min and 18 s. The image S/N was 14. (b) A 2D slice from a 3D ^{1}H Conical-SPRITE image of the same sample acquired with the same parameters as (a) except with a T_R of 250 μs. The total acquisition time was 33 s. The image S/N was 12. The displayed slice in (b) is slightly offset from the slice in (a).

has a duty cycle of 50.8% for G_x, and 100.0% for G_y and G_z during the most demanding line acquired at the edge of k-space. In Conical-SPRITE G_x and G_y are ramped sinusoidally while G_z is ramped in a stepped linear fashion. For the period of the most demanding conical acquisition, the cone at approximately 45° to the k_xk_y-plane, the duty cycle for G_x is 27.2%, G_y is 27.4%, and G_z is 46.6%. Thus for both the shorter timescale within a single experiment and for a timescale including an entire experiment, centric scan SPRITE techniques have a much lower gradient duty cycle than standard SPRITE techniques.

The gradient duty cycles considered above were calculated based on the gradient strength or gradient current; however, the gradient duty cycle can also be considered in terms of the gradient power deposition. The power output is proportional to the square of the current thus in the case of power output, the gradient duty cycle reductions from standard SPRITE to Conical-SPRITE will be even more significant. Imaging experiments which cause significant gradient overheating in standard SPRITE experiments are typically executed with minimal gradient heating in Conical-SPRITE experiments.

4.4. Passive spoiling of transverse magnetization

Residual transverse magnetization due to previous RF pulses may result in the formation of echoes and lead to image artifacts. In systems where T_2^* is less than or comparable to the gradient step length ($\sim T_R$) the residual magnetization is efficiently suppressed by "passive spoiling" due to the phase encoding gradients [4,7]. In standard SPRITE active spoiling is usually required only when sampling around the center of k-space when $\gamma\Delta G_x L_x T_R \ll 2\pi$ and $T_R = T_2^*$ [2]. The spoiling gradient strength in such cases has been discussed by Hennig [19]. The centric scan SPRITE strategies have an inherent spoiling advantage due to sampling along spiral like k-space trajectories. Each trajectory begins at the origin of k-space, where $G_x = G_y = G_z = 0$ G/cm. The gradients increase in amplitude and are never all equal to zero as k-space is traversed to the extremity of k-space. Artifacts due to unwanted echoes have not yet been observed with our centric scan SPRITE methods.

4.5. Longitudinal magnetization evolution and image blurring

We now consider the effects of longitudinal magnetization evolution during a centric scan SPRITE experiment and return to the resolution effects of increasing the RF flip angle observed in Fig. 8. Using the notation of Mastikhin et al. [7] the available longitudinal magnetization after n pulses, when magnetization preparation is not introduced, can be written as

$$M_{z,n}(T_R) = M_0(1-w)\cos^n\theta e^{-nT_R/T_1} + M_0 w, \tag{23}$$

where

$$w = \frac{1-e^{-T_R/T_1}}{1-\cos\theta e^{-T_R/T_1}}. \tag{24}$$

Longitudinal magnetization depends on two terms. The first term represents the evolution of z-magnetization during a SPRITE acquisition and depends on the number of applied RF pulses. This term influences image resolution while the second term is the steady-state term and it affects image S/N [7]. The exponential term in Eq. (23) can be further written as

$$\cos^n\theta e^{-n(T_R/T_1)} = e^{-n(T_R/T_{1app})},$$
$$\frac{1}{T_{1app}} = \frac{1}{T_1} - \frac{\ln(\cos\theta)}{T_R}. \tag{25}$$

The transient term in Eq. (25) is an exponential which depends on an apparent T_1 which incorporates flip angle effects and the natural lifetime T_1 [7,18].

Excluding the effects of diffusion during the centric scan SPRITE acquisition the MR image resolution is affected by a finite sampling function $U(t)$ and a function $R(t)$ which represents the effects of longitudinal magnetization saturation through repetitive RF pulses. $R(t)$ is dependent on the number of RF pulses and is proportional to the transient term presented in Eq. (23). The Fourier transforms of $U(t)$ and $R(t)$ yield the sampling point spread function (SPSF) and the evolution point spread function (EPSF). The sampled image, including effects of finite sampling and relaxation behavior, is given by

$$M(x,y) = F\{M(k_x,k_y)U(t)R(t)\}, \tag{26}$$

where $F\{\ \}$ denotes the Fourier transform and $M(k_x,k_y)$ is the sample magnetization in the absence of relaxation/saturation effects. The previous equation can also be written as

$$\begin{aligned} M(x,y) &= F\{M(k_{,x}k_y)\} \otimes F\{U(t)\} \otimes F\{R(t)\} \\ &= F\{M(k_x,k_y)\} \otimes SPSF \otimes EPSF \end{aligned} \tag{27}$$

which explicitly states that the actual image is a convolution with the points spread functions defined above.

We can explore the effects of the sampling function and the longitudinal magnetization relaxation function through simulation of these point spread functions. A composite PSF, which is the convolution of the SPSF and the EPSF, was calculated for a single spiral acquisition with a T_R/T_1 of 0.5% and a flip angle of 5°. Fig. 10a depicts the product of sampling function, $U(t)$, and the magnetization evolution function, $R(t)$, in k-space. The T_{1app} decay, as described by Eq. (25), is 'wrapped' around the spiral trajectory, settling into a steady state, Eq. (24), away from the centre of k-space. The Fourier transform of this function is the composite PSF and is shown in Fig. 10b.

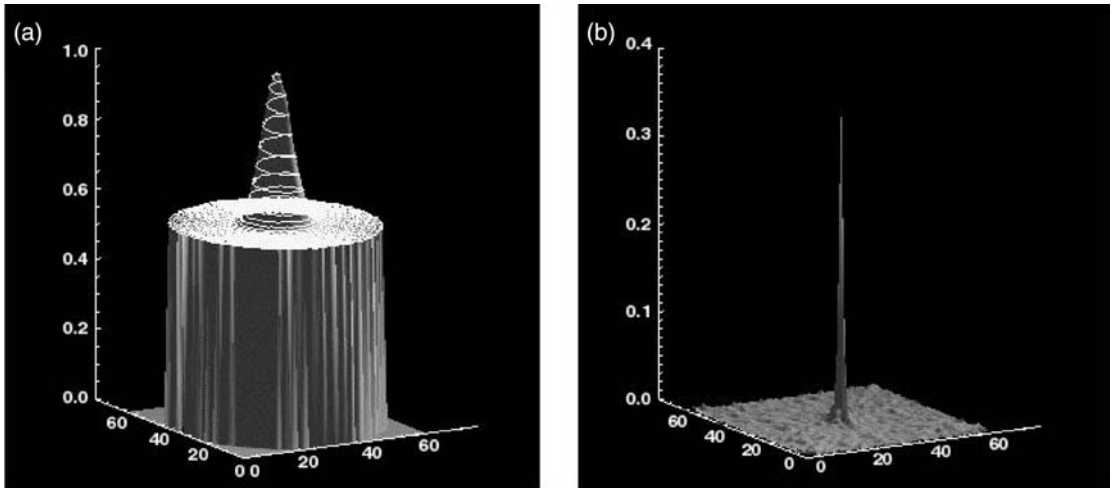

Fig. 10. (a) A numerical simulation of the product of the sampling function, $U(t)$, and the longitudinal magnetization evolution function, $R(t)$, in k-space for a single spiral, $T_R/T_1 = 0.5\%$ and flip angle = 5°. The T_{1app} decay of the longitudinal magnetization is 'wrapped' around the spiral sampling function, settling into a steady state displaced from k-space origin. The x and y coordinates are k-space points. (b) A numerical simulation of the composite PSF in image space. This is the 2D FFT of the function in (a). The x and y coordinates are x and y pixels. The PSF has a Lorentzian-like shape with additional low lying structure arising from the points omitted from the central region of k-space during the spiral trajectory. The width of the Lorentzian peak indicates the extent of convolution blurring in an analogous imaging experiment.

Mastikhin et al. [7] demonstrated that for half k-space centric scan SPRITE sampling the exponential decay of longitudinal magnetization leads to exponential filtering along the primary phase encode direction of k-space. The exponential filtering effect introduces a convolution blurring to the image in a fashion similar to the application of an exponential filter during image processing. The Fourier transform of the evolution function yields a point spread function that has a Lorentzian shape and the convolution effect leads to blurring of the image along one direction in image space [7]. The exponential filtering effect combined with the sampling methods in Spiral-SPRITE, and similarly in Conical-SPRITE, leads to a more radially symmetric composite PSF with some low lying structure due to the k-space points omitted during the spiral acquisition (Fig. 10b). The extent to which this filtering affects image resolution can be controlled by the choice of T_R and the flip angle. The flip angle is a natural choice for the control variable. Fig. 11a shows the sampling function and longitudinal magnetization evolution function in k-space for a single spiral with T_R/T_1 of 0.5% and a flip

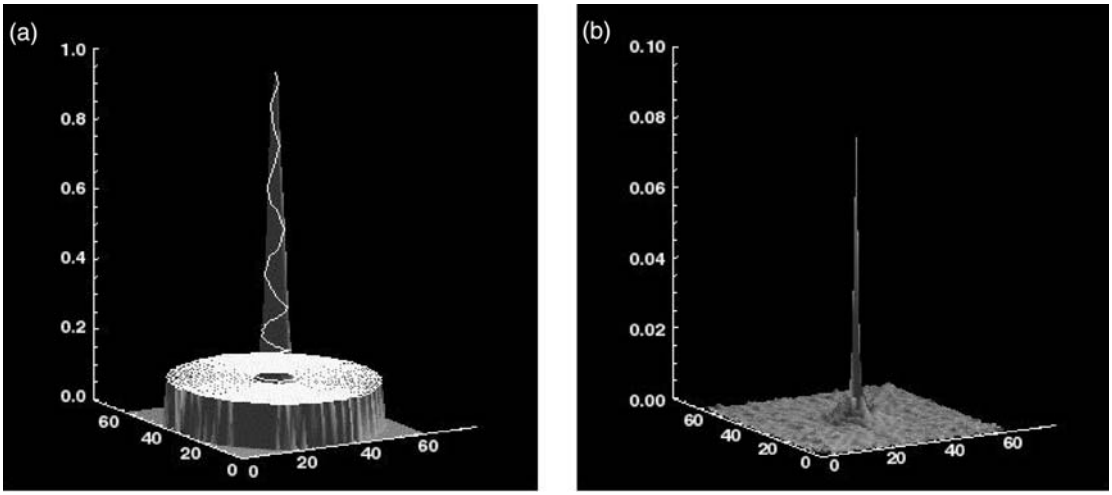

Fig. 11. (a) A numerical simulation of the product of the sampling function, $U(t)$, and the longitudinal magnetization evolution function, $R(t)$, in k-space for a single spiral, $T_R/T_1 = 0.5\%$ and flip angle = 15°. The T_{1app} decay of the longitudinal magnetization is 'wrapped' around the spiral sampling function, settling into a reduced steady state displaced from the k-space origin. (b) A numerical simulation of the composite PSF in image space. This is the 2D FFT of the function in (a). The base of the composite PSF is broader than the 5° flip angle case in Fig. 10b. This leads to increased convolution blurring in the image.

angle of 15°. The corresponding composite PSF in image space is shown in Fig. 11b. The width of the PSF is noticeably increased which would result in increased convolution blurring in the corresponding images.

The Conical-SPRITE trajectory is inherently 3D and therefore presenting a sensible geometrical representation of the 4D composite PSF for this case is problematic. However the features of the simulations presented for the 2D spiral case are representative of those for the 3D conical case. The Conical-SPRITE ^{1}H resolution phantom images presented in Fig. 8 demonstrate experimentally the convolution blurring effect of an increased flip angle. The convolution blurring of the image in Fig. 8d, with a flip angle of 13.1°, is clearly greater than that of the image in Fig. 8a, with a flip angle of 4.6°. Further investigation of the features of the composite PSF and the segregation of the effects of the SPSF and the EPSF in order to accurately predict the convolution blurring effects for both the spiral and the conical trajectory cases is the subject of ongoing research.

5. Conclusion

The pure phase encode, centric scan, techniques Spiral-SPRITE, and Conical-SPRITE are well suited to the study of a wide variety of short T_2^* systems. Both methods allow one to rationally control image intensity and spatial resolution. Both methods feature a simplification of image contrast, and an increased sensitivity compared to standard SPRITE methods. The increase in sensitivity is achieved through an increase in the raw S/N and a simultaneous decrease in acquisition time. Gradient heating concerns associated with conventional SPRITE imaging techniques are significantly reduced due to the reduced gradient duty cycles associated with the spiral and conical trajectories. Spiral and cones trajectories are readily implemented because the sampled k-space data points fall on a Cartesian grid. This removes any need for re-gridding prior to image reconstruction.

Acknowledgments

B.J.B. thanks NSERC of Canada for operating and equipment grants in addition to a Steacie fellowship (2000–2002). B.J.B. also thanks the Canada Chairs program for a Research Chair in MRI of Materials (2002–2009). D.J.G. and M.H. thank NSERC of Canada for post-graduate scholarships. The authors gratefully thank DuPont Canada for an Aid to Education award, 3M Canada for financial support, and the Teflon sample of Fig. 6. We thank R.P. MacGregor for his technical assistance.

References

[1] B.J. Balcom, SPRITE imaging of short relaxation time nuclei, in: P. Blü mler, B. Blümich, R. Botto, E. Fukushima (Eds.), Spatially Resolved Magnetic Resonance, Wiley-VCH, Toronto, 1998, pp. 75–86.
[2] C.B. Kennedy, B.J. Balcom, I.V. Mastikhin, Three-dimensional magnetic resonance imaging of rigid polymeric materials using single-point ramped imaging with T_1 enhancement (SPRITE), Can. J. Chem. 76 (1998) 1753–1765.
[3] S.D. Beyea, B.J. Balcom, P.J. Prado, A.R. Cross, C.B. Kennedy, R.L. Armstrong, T.W. Bremner, Relaxation time mapping of short T_2^* nuclei with single-point imaging methods, J. Magn. Reson. 135 (1998) 156–164.
[4] P.J. Prado, B.J. Balcom, I.V. Mastikhin, A.R. Cross, R.L. Armstrong, A. Logan, Magnetic resonance imaging of gases: a single-point ramped imaging with T_1 enhancement (SPRITE) study, J. Magn. Reson. 137 (1999) 324–332.
[5] S. Gravina, D.G. Cory, Sensitivity and resolution of constant-time imaging, J. Magn. Reson. A 104 (1994) 53–61.
[6] B.J. Balcom, R.P. MacGregor, S.D. Beyea, D.P. Green, R.L. Armstrong, T.W. Bremner, Single-point ramped imaging with T_1 enhancement (SPRITE), J. Magn. Reson. A 123 (1996) 131–134.
[7] I.V. Mastikhin, B.J. Balcom, P.J. Prado, C.B. Kennedy, SPRITE MRI with prepared magnetization and centric k-space sampling, J. Magn. Reson. 136 (1999) 159–168.
[8] D.E. Axelson, A. Kantzas, T. Eads, Single point ^{1}H magnetic resonance imaging of rigid solids, Can. J. Appl. Spectrosc. 40 (1995) 16.
[9] D.J. Goodyear, Development of single point spiral scan imaging: Spiral-SPRITE, M.Sc. Thesis, Univeristy of New Brunswick, 2000.
[10] P. Szomolanyi, D. Goodyear, B. Balcom, D. Matheson, SPIRAL-SPRITE: a rapid single point MRI technique for application to porous media, Magn. Reson. Imaging 19 (2001) 423–428.
[11] M. Halse, Conical-SPRITE: a rapid, 3D MRI method for imaging solid-like materials, B.Sc. Thesis, University of New Brunswick, 2002.
[12] P. Irarrazabal, D. Nishimura, Efficient k-space trajectories for fast three-dimensional imaging, in: Proceedings of the SMR, Second Scientific Meeting and Exhibition, San Francisco, 1994, p. 30.
[13] J. Jackson, C. Meyer, D. Nishimura, A. Macovski, Selection of a convolution function for Fourier inversion using gridding, IEEE Trans. Med. Imaging MI-10 (1991) 473–478.
[14] K.F. King, T.K.F. Foo, C.R. Crawford, Optimized gradient waveforms for spiral scanning, Magn. Reson. Med. 34 (1995) 156–160.
[15] C.B. Ahn, J.H. Kim, Z.H. Cho, High-speed spiral-scan echo planar NMR imaging—I, IEEE Trans. Med. Imaging MI-5 (1) (1986) 1–7.
[16] C.H. Meyer, A. Macovski, Square spiral fast chemical shift imaging, Magn. Reson. Imaging 5 (1987).
[17] P.T. Callaghan, Principles of Nuclear Magnetic Resonance Microscopy, Clarendon Press, Oxford, 1991.
[18] M.T. Vlaardingerbroek, J.R. den Boer, Magnetic Resonance Imaging, Springer, New York, 1996.
[19] J. Hennig, Echoes—how to generate, recognize, use or avoid them in MR-imaging sequences, Concepts Magn. Reson. 3 (1991) 125.